^{18}F-FDG Kinetics Parameters Depend on the Mechanism of Injury in Early Experimental Acute Respiratory Distress Syndrome

Nicolas de Prost[1,2], Yan Feng[1], Tyler Wellman[1,3], Mauro R. Tucci[1,4], Eduardo L. Costa[1,4], Guido Musch[1], Tilo Winkler[1], R. Scott Harris[5], Jose G. Venegas[1], Wei Chao[1], and Marcos F. Vidal Melo[1]

[1]Department of Anesthesia, Critical Care and Pain Medicine, Massachusetts General Hospital, Harvard Medical School, Boston, Massachusetts; [2]Medical Intensive Care Unit, Hôpital Henri Mondor, Assistance Publique—Hôpitaux de Paris, Créteil, France; [3]Department of Biomedical Engineering, Boston University, Boston, Massachusetts; [4]Pulmonary Division, Cardio-pulmonary Department, Heart Institute (Incor), University of São Paulo, São Paulo, Brazil; and [5]Department of Medicine (Pulmonary and Critical Care Unit), Massachusetts General Hospital, Harvard Medical School, Boston, Massachusetts

PET with ^{18}F-FDG allows for noninvasive assessment of regional lung metabolism reflective of neutrophilic inflammation. This study aimed at determining during early acute lung injury whether local ^{18}F-FDG phosphorylation rate and volume of distribution were sensitive to the initial regional inflammatory response and whether they depended on the mechanism of injury: endotoxemia and surfactant depletion. **Methods:** Twelve sheep underwent homogeneous unilateral surfactant depletion (alveolar lavage) and were mechanically ventilated for 4 h (positive end-expiratory pressure, 10 cm H_2O; plateau pressure, 30 cm H_2O) while receiving intravenous endotoxin (lipopolysaccharide-positive [LPS+] group; $n = 6$) or not (lipopolysaccharide-negative group; $n = 6$). ^{18}F-FDG PET emission scans were then acquired. ^{18}F-FDG phosphorylation rate and distribution volume were calculated with a 4-compartment model. Lung tissue expression of inflammatory cytokines was measured using real-time quantitative reverse transcription polymerase chain reaction. **Results:** ^{18}F-FDG uptake increased in LPS+ ($P = 0.012$) and in surfactant-depleted sheep ($P < 0.001$). These increases were topographically heterogeneous, predominantly in dependent lung regions, and without interaction between alveolar lavage and LPS. The increase of ^{18}F-FDG uptake in the LPS+ group was related both to increases in the ^{18}F-FDG phosphorylation rate ($P < 0.05$) and to distribution volume ($P < 0.01$). ^{18}F-FDG distribution volume increased with infiltrating neutrophils ($P < 0.001$) and phosphorylation rate with the regional expression of IL-1β ($P = 0.026$), IL-8 ($P = 0.011$), and IL-10 ($P = 0.023$). **Conclusion:** Noninvasive ^{18}F-FDG PET-derived parameters represent histologic and gene expression markers of early lung injury. Pulmonary metabolism assessed with ^{18}F-FDG PET depends on the mechanism of injury and appears to be additive for endotoxemia and surfactant depletion. ^{18}F-FDG PET may be a valuable imaging biomarker of early lung injury.

Key Words: respiratory distress syndrome, adult; endotoxemia; pulmonary edema; positron emission tomography; fluorodeoxyglucose F18

J Nucl Med 2014; 55:1871–1877
DOI: 10.2967/jnumed.114.140962

Simon et al. recognized in 1947 that the injured lung is metabolically distinct from the normal lung (*1*). Lung neutrophilic infiltration, mediated by cytokines secreted at the site of inflammation by activated endothelial and epithelial cells and leukocytes, is a key feature of the acute respiratory distress syndrome (ARDS) (*2*) and a major component of that metabolic change (*3–5*).

We and others have explored the uptake of the glucose analog ^{18}F-FDG as a biomarker of ARDS (*5–7*). For this, we applied a 4-compartment model to pulmonary ^{18}F-FDG kinetics (*8,9*), which allows for the separation of the net uptake rate of the glucose analog ^{18}F-FDG (K_i) into more specific and biologically relevant parameters: the cellular metabolic activity (phosphorylation rate constant, k_3) and the distribution volumes of tracer available for phosphorylation (F_{ei}) and in pulmonary edema (F_{ee}) (*8,9*). Indeed, k_3 has been associated with tissue hexokinase activity (*10*), tumor aggressiveness, and response to therapy (*11*) and F_{ee} with lung water content (*9*). Yet, the relationship of these more specific measures of cellular metabolic activity with regional inflammation in early lung injury is currently unknown.

Human ARDS usually results from multiple injurious hits to the lung. These hits are expected to produce different degrees of cellular metabolic activity, pulmonary edema, and ^{18}F-FDG tracer distribution. Indeed, endotoxemia produces marked tissue neutrophilic infiltration with substantial cellular activation (*12*) as well as hexokinase activation and translocation from the cytoplasm to the perimembrane region (*13*), whereas surfactant depletion by lung lavage produces discrete neutrophilic infiltration (*7,14*) with unknown effects on hexokinase. Knowledge is scant on the specific contributions of metabolic activity and tracer distribution to ^{18}F-FDG uptake in different forms of acute lung injury, their topographic distribution in heterogeneous lungs of size comparable to the human, and the regional association of those metabolic changes with gene expression of inflammatory cytokines during early lung injury.

In this study, we aimed to investigate topographically the functional, metabolic, and inflammatory changes occurring in the early stages of lung injury produced by a combination of distinct injurious mechanisms including surfactant depletion, mechanical ventilation, and endotoxemia in a large-animal model with lung heterogeneity compatible with that of humans. We also correlated the metabolic changes assessed noninvasively by imaging and

Received Apr. 1, 2014; revision accepted Aug. 8, 2014.
For correspondence or reprints contact: Nicolas de Prost, Service de Réanimation Médicale, Hôpital Henri Mondor, Assistance Publique—Hôpitaux de Paris, Créteil, France.
E-mail: nicolas.de-prost@hmn.aphp.fr
Published online Oct. 6, 2014.

modeling of pulmonary ^{18}F-FDG kinetics with regional RNA expression of cytokines usually associated with ARDS.

MATERIALS AND METHODS

Methods are further described in the supplemental material (available at http://jnm.snmjournals.org).

Experimental Protocol

The procedures were approved by the Subcommittee on Research Animal Care of the Massachusetts General Hospital. Twelve sheep (weight ± SD, 22.0 ± 1.8 kg) were anesthetized, intubated, and mechanically ventilated. A left-sided double-lumen endobronchial tube was placed through a tracheotomy and used to produce lung surfactant depletion by alveolar saline lavage. Warm saline (~400 mL) was instilled in the left bronchus (pressure, ~30 cm H_2O) of initially supine sheep, followed by draining to gravity. After 3 aliquots, animals were turned prone for 3 additional aliquots. A regular endotracheal tube was then placed and double-lung ventilation resumed.

Animals were positioned supine in the PET scanner with the field of view immediately above the diaphragmatic dome and mechanically ventilated for 4 h using the following parameters: positive end-expiratory pressure, 10 cm H_2O; fraction of inspired oxygen (FiO_2), 0.6; inspiratory-to-expiratory ratio, 1:2; tidal volume adjusted to a plateau pressure of 30 cm H_2O; and respiratory rate adjusted to normocapnia. Transmission and ^{13}NN emission PET scans were obtained at baseline and at 4 h of mechanical ventilation. ^{18}F-FDG PET scans were acquired after the 4-h ^{13}NN scan. After baseline imaging, 6 sheep (lipopolysaccharide-positive [LPS+] group) received a continuous 10 $ng \cdot kg^{-1} \cdot min^{-1}$ intravenous infusion of endotoxin (*Escherichia coli* O55:B5; List Biologic Laboratories Inc.) whereas 6 did not (LPS-negative [LPS−] group).

PET Imaging Protocol and Processing

Images consisted of 15 transverse slices. Three scan modalities were performed.

Transmission scans were acquired for attenuation correction and calculation of the gas fraction (F_{gas}) from regional tissue density (F_{tissue}):

$$F_{gas} = 1 - F_{tissue}. \quad \text{Eq. 1}$$

^{13}NN emission scans were acquired after a bolus injection of ^{13}NN-saline to measure regional pulmonary perfusion and shunt (*15*) and after inhalation of ^{13}NN-gas to measure regional ventilation (*16*). ^{18}F-FDG emission scans were obtained for quantification of regional ^{18}F-FDG kinetics. Acquisition of sequential PET frames started simultaneously with the beginning of an intravenous constant-flow 60-s infusion of ^{18}F-FDG (185–370 MBq [5–10 mCi]) and lasted 75 min. Each lung was divided for analysis into 3 adjacent isogravitational regions of interest (ROIs) of equal vertical height (nondependent, middle, and dependent).

^{18}F-FDG Kinetics

A 4-compartment model designed to quantify ^{18}F-FDG kinetics during lung injury was used to estimate kinetics parameters (Supplemental Fig. 1) (*8*). The rate constant k_3 characterizes ^{18}F-FDG phosphorylation (*17*). Two functionally distinct volumes of distribution were computed: F_{ei}, containing ^{18}F-FDG immediately available for phosphorylation, and F_{ee}, containing ^{18}F-FDG not immediately available for phosphorylation, presumably associated with lung edema (*8*). Parameters were estimated in each ROI by fitting the kinetics using an iterative optimization technique. The net uptake rate of ^{18}F-FDG from plasma to tissue (K_i) was computed as:

$$K_i = F_{ei} \times k_3. \quad \text{Eq. 2}$$

A tissue fraction, blood fraction, and wet-to-dry ratio (w/d) normalized K_i (K_{iT}) were calculated to account for the effects of regional lung aeration, blood volume, and water on ^{18}F-FDG uptake (*7*).

Lung Neutrophil Counts, Histology, and Cytokines

Five-micrometer-thick tissue samples were stained with hematoxylin and eosin for light microscopy. Regional lung expression of tumor necrosis factor α (TNF-α), IL-1β, IL-6, IL-8, and IL-10 was measured using real-time quantitative reverse transcription polymerase chain reaction (Supplemental Table 1). Neutrophil counts, acute lung injury scores (*18*), and lung cytokine expressions were assessed in nondependent (ventral) and dependent (dorsal) regions of each lung.

Statistical Analysis

Data are expressed as mean ± SD if normally distributed or median (interquartile range [IQ], 25%–75%) otherwise. Two-way ANOVA with repeated measures was used to compare physiologic values at baseline and 4 h of mechanical ventilation and compare PET data at baseline and 4 h of mechanical ventilation and between lungs. Bonferroni-corrected post hoc tests were performed when the overall P value was less than 0.05 to identify statistically significant 2 × 2 comparisons. The relationship between ^{18}F-FDG kinetics parameters and regional lung cytokine expression and neutrophil counts was assessed by linear regression.

RESULTS

Global Physiologic Variables

PaO_2/FiO_2 ratios were lower than 300 mm Hg in both groups at 4 h of mechanical ventilation. Systemic blood pressure remained stable (Table 1), whereas mean pulmonary artery pressure and pulmonary vascular resistances increased in the LPS+ group. At 4 h, the LPS+ group showed lower respiratory system compliance than the LPS− group. Blood neutrophil counts decreased markedly in the LPS+ group whereas they increased in the LPS− group (Fig. 1).

Global and Regional Gas Fraction, Shunt Fraction, and Perfusion

At 4 h of mechanical ventilation, whole-lung aeration (F_{gas}) was 30% lower in lavaged lungs and tended to be lower in the LPS+ group (Table 2). The LPS+ group presented lower F_{gas} in dependent regions than the LPS− group ($P < 0.05$), and lavaged lungs had lower F_{gas} than nonlavaged lungs ($P < 0.001$) (Fig. 2A).

LPS infusion and alveolar lavage increased whole-lung shunt fraction (Table 2). Shunt increased with LPS administration in both lavaged ($P < 0.01$) and nonlavaged lungs ($P < 0.05$) and from nondependent to dependent ROIs ($P < 0.001$) (Fig. 2B). Vertical shunt gradients were larger in the LPS+ than in the LPS− group (LPS infusion × ROI interaction, $P < 0.001$). Regional shunt was higher in lavaged than nonlavaged lungs in both groups (Fig. 2B).

Remarkably, the apparent effect of LPS on shunt contrasted with its lack of detectable effect on the distribution of lung perfusion to the whole lavaged versus nonlavaged single lungs (Table 2). At the regional level, perfusion fraction was also not affected by LPS ($P = 0.61$) (Fig. 2C) but was lower in dependent lavaged lungs in the LPS+ and LPS− groups and increased from nondependent to dependent regions ($P < 0.001$). Lavaged lungs presented lower vertical perfusion gradients than nonlavaged lungs (lavage × ROI interaction, $P < 0.001$), with dependent ROIs exhibiting approximately 30% lower perfusion fraction in lavaged than in nonlavaged lungs in both groups ($P < 0.001$).

Global and Regional Pulmonary ^{18}F-FDG Kinetics

Metabolic activity quantified by the net ^{18}F-FDG uptake rate K_i was higher in lavaged and LPS-exposed lungs after 4 h of

TABLE 1
Global Physiologic Variables at Baseline (After Unilateral Lung Lavage) and After 4 Hours of Mechanical Ventilation

Variable	LPS−		LPS+		*P*	
	Baseline (n = 6)	4 h (n = 6)	Baseline (n = 6)	4 h (n = 6)	Time	LPS
V_T (mL/kg)	15.7 ± 5.6	16.6 ± 4.7	13.4 ± 3.5	11.8 ± 2.7	0.63	0.16
PEEP (cm H_2O)	10 (10–11)	10 (9–11)	9 (8–10)	9 (8–10)	0.73	0.18
Respiratory rate (/min)	23 ± 4	23 ± 4	21 ± 5	21 ± 4	0.66	0.33
Pa_{O2}/FiO_2 (torr)	149 (102–320)	161 (123–173)	109 (84–300)	89 (64–211)	0.92	0.37
Pa_{CO2} (torr)	33 ± 5	37 ± 7	36 ± 10	39 ± 4	0.20	0.38
Crs (mL/cm H_2O)	17.4 ± 6.3	18.6 ± 4.1	13.3 ± 3.5	11.2 ± 3.1*	0.65	0.03
Qs/Qt	0.32 (0.18–0.48)	0.35 (0.11–0.56)	0.43 (0.23–0.53)	0.56 (0.23–0.66)	0.28	0.26
PVR (dynes·s·cm^{-5})	393 ± 99	314 ± 84	253 ± 82†	584 ± 163‡	<0.001	0.07
MPAP (mm Hg)	22 ± 2	22 ± 4	22 ± 5†	34 ± 5‡	<0.001	0.02
MAP (mm Hg)	102 ± 12	98 ± 18	84 ± 8	84 ± 23	0.77	0.04
Heart rate (bpm)	155 ± 43	157 ± 41	185 ± 29	167 ± 29	0.54	0.26
Cardiac output (L/min)	4.1 ± 1.3	3.3 ± 0.5	4.7 ± 0.8	3.7 ± 0.7	0.02	0.24

*$P < 0.05$ vs. LPS− group at 4 h of mechanical ventilation and LPS (mechanical ventilation + LPS).
†$P < 0.001$ vs. 4 h of mechanical ventilation + LPS for same group.
‡$P < 0.001$ vs. LPS− group at 4 h of mechanical ventilation and LPS (mechanical ventilation + LPS).
V_T = tidal volume; PEEP = positive end-expiratory pressure; Crs = respiratory system compliance; Qs/Qt = global shunt fraction; PVR = pulmonary vascular resistances; MPAP = mean pulmonary arterial pressure; MAP = mean arterial pressure.
Data are mean ± SD or median, with IQ (25-75) in parentheses.

mechanical ventilation (Table 2; Fig. 3). There was no statistically significant interaction between alveolar lavage and LPS, suggesting their additive rather than synergistic effect on K_i. Lavaged lungs exhibited 1.5 (IQ, 1.2–1.9) times higher K_i values than nonlavaged lungs. LPS+ lavaged lungs showed 2.6 (IQ, 1.1–5.6) times higher K_i values than LPS− lavaged lungs. Regional analysis revealed higher K_i in lavaged ($P < 0.01$) and LPS+ ($P < 0.01$) lungs (Fig. 4A). The effect of both LPS exposure and alveolar lavage on K_i interacted with ROI location ($P < 0.001$)—that is, both LPS+ and lavaged lungs presented larger ^{18}F-FDG uptake vertical gradients than LPS− and nonlavaged lungs. In dependent and middle regions, LPS+ lavaged lung K_i values were 2.5 (IQ, 2.0–6.9) and 1.7 (IQ, 1.3–3.3) times higher than those of LPS− lavaged lungs.

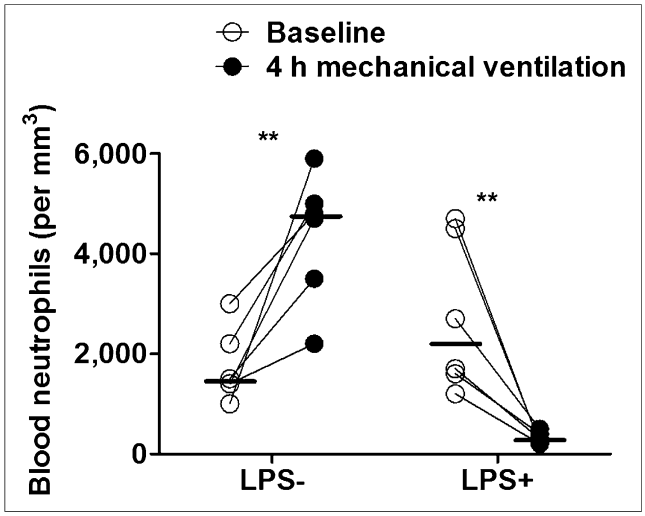

FIGURE 1. Blood neutrophil counts at baseline and 4 h of mechanical ventilation. Counts increased significantly in LPS− group, in contrast to significant decrease in LPS+ group. Horizontal lines represent median values. **$P < 0.01$.

Dependent regions of LPS+ and LPS− lavaged lungs had higher K_i values than those of nonlavaged lungs despite a 30% reduction in regional perfusion in these areas (Fig. 2C). Those significant effects of LPS administration ($P < 0.001$) and ROIs ($P < 0.05$) on ^{18}F-FDG uptake were still present when regional aeration, blood volume, and water (Supplemental Fig. 2) were accounted for (K_{iT}, Fig. 4B), indicating that they were not a mere consequence of regional changes in lung density. In contrast, there was no effect of lavage on K_{iT} ($P = 0.12$).

To understand the factors determining regional K_i, we studied its components: the phosphorylation rate (k_3) and the distribution volume of tracer immediately available for phosphorylation (F_{ei}), where $K_i = k_3 \cdot F_{ei}$. This analysis revealed that k_3 tended to increase with LPS but not with lavage (Table 2). In contrast, F_{ei} was increased by both alveolar lavage and LPS exposure (Table 2). Regional k_3 was higher in LPS+ lungs ($P < 0.05$) but not affected by lavage ($P = 0.81$) nor by ROI location ($P = 0.20$) (Fig. 4C). Regional F_{ei} was higher with LPS ($P < 0.05$) and increased from nondependent to dependent regions (Fig. 4D; $P < 0.001$), with significant interaction (LPS × ROIs; $P = 0.016$), indicating that LPS magnified the vertical gradient of F_{ei}. Regional F_{ei} was also higher in lavaged lungs of the LPS− group ($P < 0.001$) and tended to be higher in the LPS+ group ($P = 0.074$).

Regional Lung Neutrophilic Infiltration and Lung Cytokine Messenger RNA Expression

Whole-lung neutrophil counts were higher with LPS and lung lavage (Table 2). In both groups, regional neutrophil counts were higher in dependent than nondependent regions and in dependent lavaged than nonlavaged regions (Supplemental Fig. 3A). Lavaged

TABLE 2
Whole-Lung Variables at 4 Hours of Mechanical Ventilation

Variable	LPS−		LPS+		*P*		
	Nonlavaged lung	Lavaged lung	Nonlavaged lung	Lavaged lung	Lavage	LPS	Interaction
K_i (10^{-3}/min)	1.2 ± 1.0	2.3 ± 1.7*	4.4 ± 1.9	7.2 ± 4.3†	<0.01	0.012	0.20
F_{ei} (10^{-2})	7.6 ± 2.1	12.6 ± 1.4†,‡	14.7 ± 5.9	22.2 ± 8.6§	<0.001	0.015	0.32
k_3 (10^{-2}/min)	1.6 ± 1.0	1.8 ± 1.3	3.1 ± 1.6	3.6 ± 2.5	0.45	0.10	0.78
F_{gas}	0.73 ± 0.08	0.50 ± 0.18§	0.59 ± 0.06	0.41 ± 0.08§	<0.001	0.057	0.50
Perfusion fraction	0.52 ± 0.09	0.47 ± 0.09	0.56 ± 0.08	0.43 ± 0.08	0.12	0.37	0.47
Shunt	0.18 ± 0.06	0.27 ± 0.04‡	0.33 ± 0.09	0.58 ± 0.08†	0.013	0.023	0.20
Neutrophils/field	3.3 ± 1.9	4.9 ± 2.2*	4.3 ± 3.3	8.7 ± 4.5‖	<0.001	0.045	0.033

*$P < 0.01$ vs. lavaged lung of LPS+ group.
†$P < 0.05$ vs. nonlavaged lung of same group.
‡$P < 0.05$ vs. lavaged lung of LPS+ group.
§$P < 0.01$ vs. nonlavaged lung of same group.
‖$P < 0.001$ vs. nonlavaged lung of same group.

lungs of the LPS+ group exhibited 2.1 ± 1.3 times more lung neutrophils than those of the LPS− group. Lung injury score was increased by LPS both in lavaged ($P = 0.056$) and in nonlavaged ($P < 0.001$) lungs, with no effect of ROI position or lavage (Fig. 5; Supplemental Fig. 3B). LPS administration increased the pulmonary messenger RNA expression of all studied cytokines (Supplemental Fig. 4). In contrast, alveolar lavage increased only the expression of TNF-α.

The determinants of the ^{18}F-FDG uptake rate, F_{ei} and k_3, were regionally associated with lung tissue neutrophil counts and cytokine expression. F_{ei} increased with neutrophil counts in the LPS+ group ($R^2 = 0.31$, $P < 0.001$) but not in the LPS− group ($R^2 = 0.08$, $P = 0.18$) (Supplemental Fig. 5). The ^{18}F-FDG phosphorylation rate k_3 increased with the regional expression of IL-1β, IL-8, and IL-10 in the LPS+ but not in the LPS− group (Table 3; Supplemental Fig. 6).

DISCUSSION

Our study showed that exposure to mild–moderate endotoxemia led to a substantially larger lung metabolic response, assessed with ^{18}F-FDG uptake, than did surfactant depletion. The increase of ^{18}F-FDG uptake in LPS-exposed lungs derived from increases in both the phosphorylation rate k_3, a noninvasive measure of hexokinase activity, and the distribution volume of ^{18}F-FDG available for phosphorylation. In contrast, increases in ^{18}F-FDG uptake in lavaged lungs not exposed to LPS were predominantly related to increases in that distribution volume of ^{18}F-FDG. In LPS-exposed lungs, the regional k_3 was statistically albeit weakly associated with the local expression of key cytokines involved with neutrophil chemoattraction and the distribution volume of ^{18}F-FDG with the number of infiltrating neutrophils.

We used mechanical ventilation pressures bound by accepted clinical limits and 2 well-defined experimental models of ARDS: endotoxemia, which induces pulmonary vascular sequestration of neutrophils within the first hour (*19*), and surfactant depletion by alveolar lavage, known to produce mild lung neutrophilic infiltration (*7,14*). The combination of these models allowed us to investigate regional pulmonary ^{18}F-FDG kinetics and neutrophil recruitment in distinct injurious lung conditions. The contrasting response of blood neutrophil counts in LPS-exposed (decreased) versus nonexposed (increased) animals indicates that different

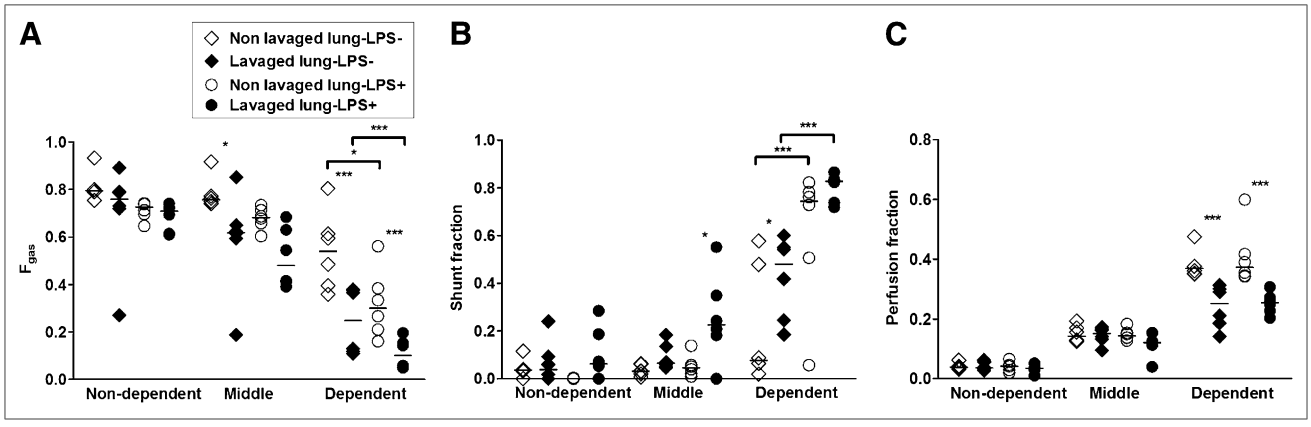

FIGURE 2. F_{gas} (A), shunt fraction (B), and perfusion fraction (C) for dependent, middle, and nondependent ROIs of lavaged and nonlavaged lungs of LPS− and LPS+ groups after 4 h of mechanical ventilation. Horizontal lines represent median values. *$P < 0.05$. ***$P < 0.001$.

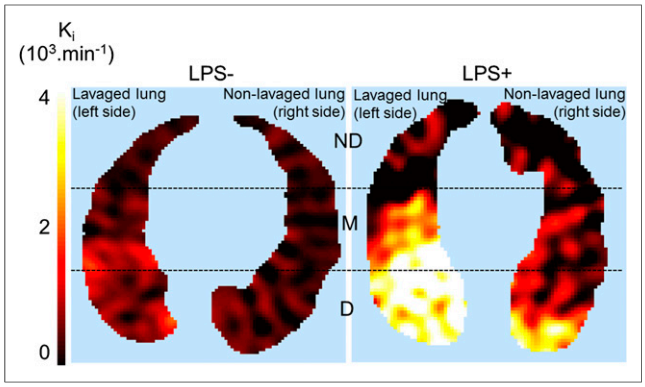

FIGURE 3. Transverse single slice of ^{18}F-FDG uptake rate (K_i, computed voxel-by-voxel with Patlak method (*28*)) in LPS+ and LPS− animal. Color scale: black = lowest, white = highest values in image. Dashed lines indicate separation among 3 isogravitational ROIs: nondependent (ND), middle (M), and dependent (D). There is higher ^{18}F-FDG uptake in lavaged than in nonlavaged lung. LPS+ lungs exhibited markedly higher ^{18}F-FDG uptake than LPS− lungs.

levels of neutrophilic inflammation were triggered. Accordingly, lung neutrophilic infiltration was increased by both insults, to a greater extent with LPS than with surfactant depletion, consistent with the finding of higher ^{18}F-FDG uptake with LPS.

Both surfactant depletion and LPS exposure increased the whole-lung net ^{18}F-FDG uptake rate K_i. K_i distribution was markedly heterogeneous within lavaged and nonlavaged lungs, following a gradient along the ventral–dorsal axis. Importantly, this gradient was still present after accounting for regional lung density, blood volume, and water content (Ki_T), emphasizing that regional differences were not merely due to lung edema or collapse (*7*). Factors potentially accounting for larger inflammation in dependent regions are mechanical instabilities exacerbated by surfactant depletion with concentration of stresses (*20*), cyclic recruitment (*7*), and vertical perfusion gradients (*6*).

K_i derives from the product of ^{18}F-FDG phosphorylation rate (k_3), representing hexokinase activity (*8,10,17,21,22*), and the distribution volume of ^{18}F-FDG immediately available for phosphorylation (F_{ei}, $K_i = k_3 \cdot F_{ei}$). Regional quantification of these K_i components revealed that the effects of LPS exposure and lavage on ^{18}F-FDG uptake differed not only by their magnitude, but also by the contribution of those components. Indeed, LPS increased ^{18}F-FDG uptake through both F_{ei} and k_3. In contrast, alveolar lavage increased ^{18}F-FDG uptake primarily through F_{ei}. Considering that neutrophils are the main cells contributing to lung ^{18}F-FDG uptake during lung injury (*5,23,24*), our in vivo data suggest that neutrophilic inflammation produced by endotoxemia is characterized not only by increased neutrophil counts but also importantly by more metabolically activated neutrophils than those during alveolar lavage. This finding is consistent with the higher injury scores found in LPS+ nonlavaged than in LPS− lavaged dependent regions, despite their similar neutrophil counts. The relevance of understanding and quantifying these components with a noninvasive technique translatable to humans is highlighted by the likely crucial role of neutrophil activation in the development of ARDS (*2*).

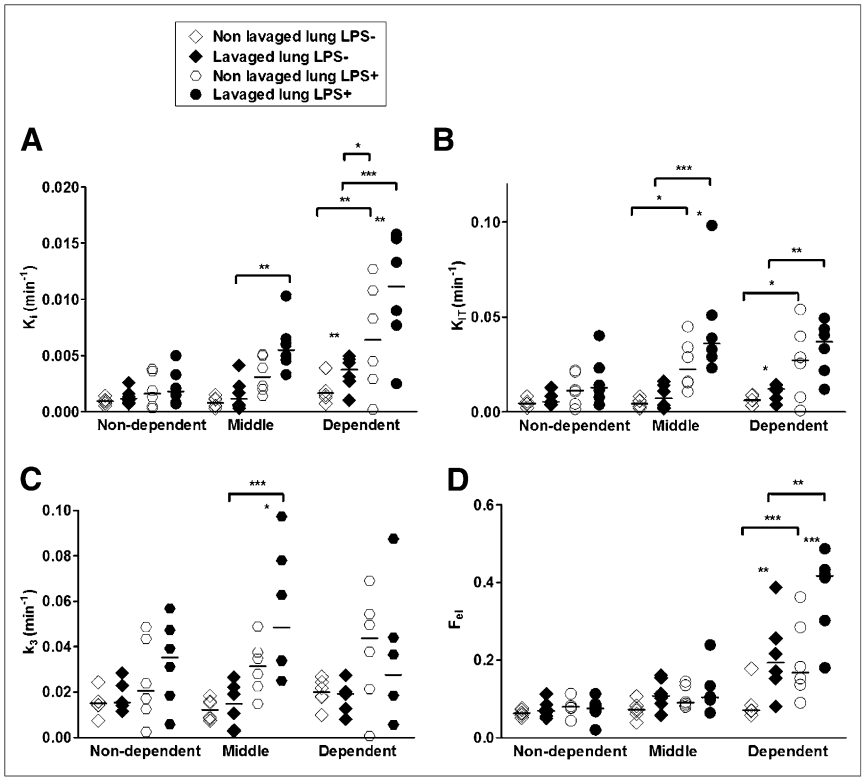

FIGURE 4. ^{18}F-FDG kinetics parameters estimated with 4-compartment model in isogravitational ROIs of lavaged and nonlavaged lungs of LPS− and LPS+ groups. ^{18}F-FDG net uptake rate (Ki) without (A) or with (Ki_T) (B) normalization for tissue density; blood volume; and w/d ratios (i.e., $Ki_T = Ki \cdot [w/d]/[F_{tissue} \cdot (w_N/d_N)]$) (where w_N/d_N is the normal w/d ratio of a sheep lung), rate constant k_3 (associated with hexokinase activity) (C), and intracellular distribution volume of ^{18}F-FDG (F_{ei}) (D). *$P < 0.05$. **$P < 0.01$. ***$P < 0.001$.

The value of k_3 as a measure of cell phosphorylation rate (*10*), and thus as a direct noninvasive assessment of cellular metabolic activity, has been explored in oncology with large k_3 values related to increased cancer aggressiveness and poor prognosis, whereas low k_3 indicated effectiveness of therapy (*10,11*). Knowledge is scant on the value of k_3 during ARDS. In sheep models of endotoxemic ARDS, higher k_3 values were observed with an injurious versus a protective mechanical ventilation strategy in dependent lung regions (*22*) and related to the magnitude of regional lung strain (*25*).

Our data indicate a weak but statistically significant association between regional k_3 and regional expression of IL-1β, IL-8, and IL-10, suggesting a relationship between the metabolic activity of neutrophils and the regional expression of neutrophil-chemoattracting cytokines. Interestingly, the cytokine with the strongest correlation with k_3 was IL-8, presumably the main neutrophil-chemoattracting cytokine during ARDS (*26*). Such findings are consistent with our measurements of increased neutrophil counts and metabolic activity in endotoxin-exposed lung. The obtained r^2 values for the k_3-cytokine gene expression association were small, suggesting

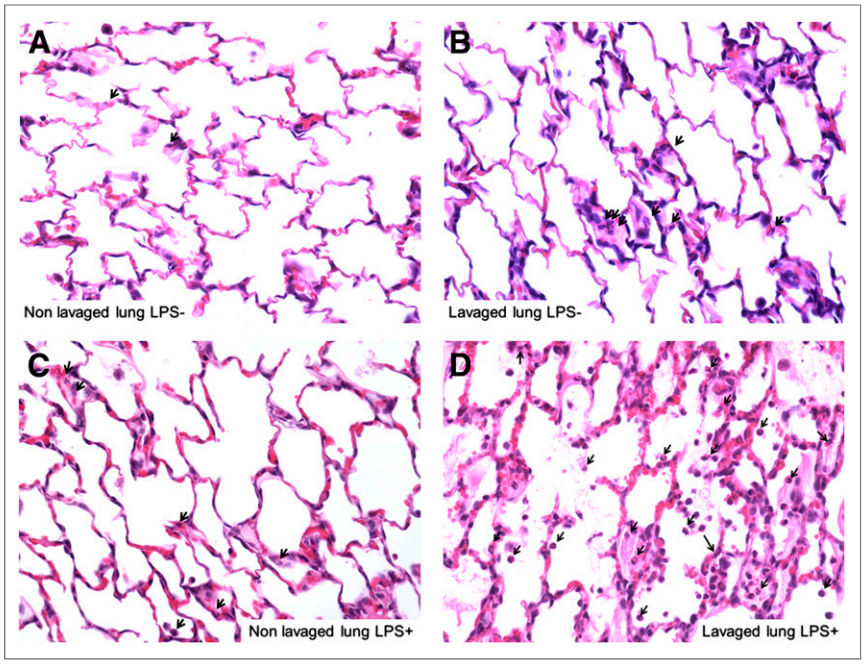

FIGURE 5. Hematoxylin and eosin–stained histologic sections of dependent (dorsal) regions of nonlavaged (A and C) and lavaged (B and D) lungs from LPS− (A and B) and LPS+ animal (C and D) (magnification, ×400). Lavaged lungs exhibited neutrophilic infiltration (arrows) and mild thickening of alveolar walls but no other feature assessed in lung injury score (i.e., capillary congestion, alveolar edema, and alveolar hemorrhage). LPS exposure produced marked neutrophilic infiltration by neutrophils as well as capillary congestion and alveolar edema, particularly in lavaged lung (D).

a relevant role for other biologic processes in determining regional k_3. Potentially relevant biologic factors present between gene expression of cytokines and tissue phosphorylation rate (k_3) include gene translation, presence of cytokine receptors and required enzymes in target areas, and time course of gene transcription and translation. Additional sources could contribute to variability such as coregistration between ROIs used to compute ^{18}F-FDG kinetics parameters and lung tissue samples (cytokines) and precision of cytokines messenger RNA measurements.

TABLE 3
Linear Regression Between Regional Lung Expression of Cytokines (TNF-α, IL-1β, IL-6, IL-8, and IL-10) and Regional Phosphorylation Rate k_3 for LPS− and LPS+ Groups

	LPS−		LPS+	
Cytokine	R^2	P	R^2	P
TNF-α	0.02	0.45	0.01	0.58
IL-1β	0.01	0.65	0.14	0.026*
IL-6	0.01	0.80	0.04	0.22
IL-8	0.01	0.93	0.18	0.011
IL-10	0.07	0.14	0.14	0.023*

*Correlation was still significant after removing outlier point (IL-1β: $R^2 = 0.15$, $P = 0.019$; IL-10: $R^2 = 0.10$, $P = 0.029$).

Coefficients of determination (R^2) and P values for correlation between k_3 and regionally measured cytokines.

In the LPS− group, however, regional F_{ei} did not correlate with lung neutrophil counts and regional k_3 did not correlate with regional lung cytokines. These findings are consistent with the mild neutrophilic infiltration produced by saline lavage (*14*) and its mild effect on cytokine expression, except for TNF-α (*27*). Interestingly, recent microautoradiography data in murine ARDS models not only confirmed predominant ^{18}F-FDG uptake in neutrophils after LPS exposure, but also revealed that type 2 pneumocytes contributed significantly to ^{18}F-FDG uptake in ventilator-induced injury (*23*). Thus, the lack of correlation between F_{ei} and lung neutrophils in LPS− animals could imply the contribution of other cell types to ^{18}F-FDG uptake (*21,23*).

Overall, our results indicate that regional ^{18}F-FDG kinetics parameters during experimental ARDS depend on the mechanism of lung injury. Similar K_i values can derive from different combinations of k_3 and F_{ei} relevant for interpretation of ^{18}F-FDG measurements. k_3 and F_{ei} allow for valuable assessment of inflammatory activity during early lung injury. In view of their noninvasiveness and human applicability, ^{18}F-FDG kinetics measurements could be considered to study and manage patients at risk for ARDS and to evaluate therapeutic strategies. The time and logistic considerations currently necessary to scan these critically ill patients limit the potential use of these techniques to selected patients.

Perfusion is a key variable in the process of regional load of inflammatory cells and mediators and consequently a potential important determinant of regional ^{18}F-FDG uptake and lung injury (*6*). However, we found that within isogravitational ROIs, perfusion fractions were similar irrespective of LPS exposure and lower in surfactant-depleted versus nondepleted lungs, implying that differences in regional perfusion could not account for the observed inter-ROI differences in ^{18}F-FDG kinetics and regional inflammatory response. Such a result is unexpected, because in heterogeneously perfused lungs, a direct relationship between inflammation and blood flow would be anticipated (*6*). The lack of direct relationship suggests that differences in ^{18}F-FDG kinetics parameters among groups, determined by glucose transport and metabolism processes, are not entirely limited by regional blood flow in the ranges of physiologic variables present in the study.

CONCLUSION

Our study shows that pulmonary metabolic activity measured in vivo and noninvasively by ^{18}F-FDG PET increased globally and regionally in response to LPS, surfactant depletion, and mechanical ventilation. The increase in metabolic activity after 4 h of mechanical ventilation was higher after moderate endotoxemia than after alveolar lavage and predominated in dependent lung regions. Pulmonary ^{18}F-FDG kinetics analysis showed that LPS increased lung metabolism through increases in both phosphorylation rate of lung tissue and the volume of distribution of ^{18}F-FDG. That phosphorylation rate was associated with the regional

gene expression of cytokines important to the regional control of neutrophil chemoattraction and the regional volume of distribution of ^{18}F-FDG with the number of infiltrating neutrophils. These findings support the application of advanced modeling of ^{18}F-FDG kinetics as an imaging-based biomarker of early lung injury.

DISCLOSURE

The costs of publication of this article were defrayed in part by the payment of page charges. Therefore, and solely to indicate this fact, this article is hereby marked "advertisement" in accordance with 18 USC section 1734. This work was supported by NIH grant HL 5R01HL086827 and 1R01HL121228. GM was supported by 5R01HL094639. No other potential conflict of interest relevant to this article was reported.

ACKNOWLEDGMENTS

We thank Dr. Florence Canoui-Poitrine for reviewing the statistical methods.

REFERENCES

1. Simon FP, Potts AM, Gerard RW. Metabolism of isolated lung tissue: normal and in phosgene poisoning. *J Biol Chem.* 1947;167:303–311.
2. Ware LB, Matthay MA. The acute respiratory distress syndrome. *N Engl J Med.* 2000;342:1334–1349.
3. Jones HA, Cadwallader KA, White JF, Uddin M, Peters AM, Chilvers ER. Dissociation between respiratory burst activity and deoxyglucose uptake in human neutrophil granulocytes: implications for interpretation of ^{18}F-FDG PET images. *J Nucl Med.* 2002;43:652–657.
4. Chen DL, Rosenbluth DB, Mintun MA, Schuster DP. FDG-PET imaging of pulmonary inflammation in healthy volunteers after airway instillation of endotoxin. *J Appl Physiol.* 2006;100:1602–1609.
5. Musch G, Venegas JG, Bellani G, et al. Regional gas exchange and cellular metabolic activity in ventilator-induced lung injury. *Anesthesiology.* 2007;106:723–735.
6. Costa EL, Musch G, Winkler T, et al. Mild endotoxemia during mechanical ventilation produces spatially heterogeneous pulmonary neutrophilic inflammation in sheep. *Anesthesiology.* 2010;112:658–669.
7. de Prost N, Costa EL, Wellman T, et al. Effects of surfactant depletion on regional pulmonary metabolic activity during mechanical ventilation. *J Appl Physiol.* 2011;111:1249–1258.
8. Schroeder T, Vidal Melo MF, Musch G, Harris RS, Venegas JG, Winkler T. Modeling pulmonary kinetics of 2-deoxy-2-[^{18}F]fluoro-D-glucose during acute lung injury. *Acad Radiol.* 2008;15:763–775.
9. Dittrich AS, Winkler T, Wellman T, et al. Modeling ^{18}F-FDG kinetics during acute lung injury: experimental data and estimation Errors. *PLoS ONE.* 2012;7:e47588.
10. Okazumi S, Isono K, Enomoto K, et al. Evaluation of liver tumors using fluorine-18-fluorodeoxyglucose PET: characterization of tumor and assessment of effect of treatment. *J Nucl Med.* 1992;33:333–339.
11. Dimitrakopoulou-Strauss A, Strauss LG, Burger C, et al. Prognostic aspects of ^{18}F-FDG PET kinetics in patients with metastatic colorectal carcinoma receiving FOLFOX chemotherapy. *J Nucl Med.* 2004;45:1480–1487.
12. Markovic N, McCaig LA, Stephen J, et al. Mediators released from LPS-challenged lungs induce inflammatory responses in liver vascular endothelial cells and neutrophilic leukocytes. *Am J Physiol Gastrointest Liver Physiol.* 2009;297:G1066–G1076.
13. Huang JB, Kindzelskii AL, Petty HR. Hexokinase translocation during neutrophil activation, chemotaxis, and phagocytosis: disruption by cytochalasin D, dexamethasone, and indomethacin. *Cell Immunol.* 2002;218:95–106.
14. Lachmann B, Robertson B, Vogel J. In vivo lung lavage as an experimental model of the respiratory distress syndrome. *Acta Anaesthesiol Scand.* 1980;24:231–236.
15. Vidal Melo MF, Layfield D, Harris RS, et al. Quantification of regional ventilation-perfusion ratios with PET. *J Nucl Med.* 2003;44:1982–1991.
16. Vidal Melo MF, Harris RS, Layfield D, Musch G, Venegas JG. Changes in regional ventilation after autologous blood clot pulmonary embolism. *Anesthesiology.* 2002;97:671–681.
17. Sokoloff L, Reivich M, Kennedy C, et al. The [^{14}C]deoxyglucose method for the measurement of local cerebral glucose utilization: theory, procedure, and normal values in the conscious and anesthetized albino rat. *J Neurochem.* 1977;28:897–916.
18. Mikawa K, Maekawa N, Nishina K, Takao Y, Yaku H, Obara H. Effect of lidocaine pretreatment on endotoxin-induced lung injury in rabbits. *Anesthesiology.* 1994;81:689–699.
19. Warner AE, DeCamp MM Jr, Molina RM, Brain JD. Pulmonary removal of circulating endotoxin results in acute lung injury in sheep. *Lab Invest.* 1988;59:219–230.
20. Mead J, Takishima T, Leith D. Stress distribution in lungs: a model of pulmonary elasticity. *J Appl Physiol.* 1970;28:596–608.
21. de Prost N, Tucci MR, Melo MF. Assessment of lung inflammation with ^{18}F-FDG PET during acute lung injury. *AJR.* 2010;195:292–300.
22. de Prost N, Costa EL, Wellman T, et al. Effects of ventilation strategy on distribution of lung inflammatory cell activity. *Crit Care.* 2013;17:R175.
23. Saha D, Takahashi K, de Prost N, et al. Micro-autoradiographic assessment of cell types contributing to 2-deoxy-2-[^{18}F]fluoro-D-glucose uptake during ventilator-induced and endotoxemic lung injury. *Mol Imaging Biol.* 2013;15:19–27.
24. Jones HA, Clark RJ, Rhodes CG, Schofield JB, Krausz T, Haslett C. In vivo measurement of neutrophil activity in experimental lung inflammation. *Am J Respir Crit Care Med.* 1994;149:1635–1639.
25. Wellman TJ, Winkler T, Costa EL, et al. Effect of local tidal lung strain on inflammation in normal and lipopolysaccharide-exposed sheep. *Crit Care Med.* 2014;42:e491–e500.
26. Donnelly SC, Strieter RM, Kunkel SL, et al. Interleukin-8 and development of adult respiratory distress syndrome in at-risk patient groups. *Lancet.* 1993;341:643–647.
27. Imai Y, Kawano T, Iwamoto S, Nakagawa S, Takata M, Miyasaka K. Intratracheal anti-tumor necrosis factor-alpha antibody attenuates ventilator-induced lung injury in rabbits. *J Appl Physiol.* 1999;87:510–515.
28. Patlak CS, Blasberg RG, Fenstermacher JD. Graphical evaluation of blood-to-brain transfer constants from multiple-time uptake data. *J Cereb Blood Flow Metab.* 1983;3:1–7.

JNM The Journal of NUCLEAR MEDICINE

^{18}F-FDG Kinetics Parameters Depend on the Mechanism of Injury in Early Experimental Acute Respiratory Distress Syndrome

Nicolas de Prost, Yan Feng, Tyler Wellman, Mauro R. Tucci, Eduardo L. Costa, Guido Musch, Tilo Winkler, R. Scott Harris, Jose G. Venegas, Wei Chao and Marcos F. Vidal Melo

J Nucl Med. 2014;55:1871-1877.
Published online: October 6, 2014.
Doi: 10.2967/jnumed.114.140962

The Journal of Nuclear Medicine is published monthly.
SNMMI | Society of Nuclear Medicine and Molecular Imaging
1850 Samuel Morse Drive, Reston, VA 20190.
(Print ISSN: 0161-5505, Online ISSN: 2159-662X)

SNMMI SOCIETY OF NUCLEAR MEDICINE AND MOLECULAR IMAGING